Economic Geology, v. 100, pp. 333–348

The Distribution of Base Metals and Platinum-Group Elements in Magnetitite and Its Host Rocks in the Rio Jacaré Intrusion, Northeastern Brazil

J. H. S. Sá,

Centro de Pesquisa em Geofísica e Geologia, Instituto de Geociências, Universidade Federal da Bahia 40.170-290 Salvador, Bahia, Brazil

S-J. Barnes,

Sciences de la Terre, Université du Quebec, 555 Boulevard de l'Université, Chicoutimi, Quebec, Canada G7H 2B1

H. M. Prichard,† and P. C. Fisher

School of Earth, Ocean and Planetary Sciences, University of Cardiff, Main College, Park Place, Cardiff CF10 3YE, United Kingdom

Abstract

Anomalously high Pt and Pd values have been found in three magnetite bodies in the Rio Jacaré intrusion of northeastern Brazil. The intrusion hosting these magnetite bodies consists predominantly of pyroxenite and gabbro. One magnetite body occurs in the Lower zone and two in the Upper zone of the intrusion. These bodies contain approximately 0.04 percent Ni, 0.1 percent Cu, 0.18 percent S, 1 ppb Ir, 3 ppb Rh, 160 ppb Pt, 120 ppb Pd, and 37 ppb Au. They are much richer in platinum-group elements (PGE) than the surrounding silicate rocks, and there are significant correlations among all of the PGE and between PGE and Ni. However the correlations between PGE and Au, Cu, and S are much weaker than correlations between Au, Cu, and S.

In the magnetite bodies palladium-rich minerals, especially bismuthides and antimonides, are the most abundant platinum-group minerals (PGM). In most cases these occur with interstitial silicates or within silicate inclusions in magnetite and ilmenite grains and are associated with Co-bearing pentlandite and in a few cases with Co-Ni sulfarsenides and arsenides. Sperrylite ($PtAs_2$) is the most abundant Pt mineral and is associated with silicates interstitial to magnetite and ilmenite grains and sometimes with Co-Ni arsenides. At sites where the igneous mafic minerals have been altered to amphiboles, sperrylite may be altered to Pt-Fe alloys. Other alloys present include Pd-Sn-Cu, Pt-Cu, Pt-Ni, and Pt-Au.

It is suggested that Ni and PGE were concentrated in the magnetite bodies by the coprecipitation of a small quantity of sulfide with the magnetite. These PGE-bearing base metal sulfides subsequently exsolved PGM. The association of Pd minerals with base metal sulfides and the small variation in the Pt/Pd ratio (ca. 1.4) suggests that the PGE have not been extensively remobilized in the magnetitite. In contrast, the strong correlation between S, Cu, and Au suggests that, in addition to the redistribution of S, it is likely that Cu and Au were remobilized. It is not possible to say whether the redistribution of sulfur was due to late magmatic fluids dissolving S or the later metamorphic events.

The association of PGE enrichment with magnetite layers in the Rio Jacaré intrusion contrasts with that of the Bushveld, Stillwater, Great Dyke, and Munni Munni Complexes. In these complexes PGE-enriched layers or reefs are found in the lower third of the complexes and the oxide associated with the reefs is chromite. Magnetite-bearing layers, which form from an evolved magma in the upper parts of the intrusions, are generally barren of PGE because, at the time of magnetite crystallization, the PGE had already precipitated either in sulfides or PGM. However in a number of intrusions (e.g., Rincon del Tigre, Skaergaard, Stella, and Rio Jacaré) the upper magnetite-bearing portion of the intrusion shows PGE enrichment. This enrichment is rarely associated with visible sulfides but suggests a possible new target for PGE exploration.

Introduction

In the 1970s and early 1980s the Rio Jacaré intrusion was investigated by geologic mapping and geochemical and geophysical prospecting, mainly by Companhia Baiana de Pesquisa Mineral (CBPM), a mineral development company owned by the state of Bahia's Secretary of Industry, Commerce and Mining. As a result of these investigations reserves of 6.1 million tons (Mt) of magnetitite with an average grade of 1.27 percent V_2O_5 were outlined in the Rio Jacaré intrusion (Galvão et al., 1986).

In a reconnaissance study Sá (1985, unpub. report for Companhia Baiana de Pesquisa Mineral, Salvador, Brazil) established that some samples of pyroxenite and magnetitite from the Rio Jacaré intrusion contain approximately 300 ppb Pt and 110 ppb Pd. These results encouraged further investigation to determine in detail the distribution of the platinum-group elements (PGE) in these rocks. This paper describes the PGE distribution and the platinum-group minerals (PGM) present within the Rio Jacaré intrusion, their relationship to the magnetitite, and the effects of magmatic, and subsequent alteration processes on the PGE. In this study, the term magnetitite is used for a rock in which Fe-Ti oxides make up more than 70 percent of the rock; larger scale features containing magnetitite and rock types with less than 70 percent magnetite but more than 10 percent magnetite are referred to as magnetite bodies or lenses.

† Corresponding author: e-mail, Prichard@cardiff.ac.uk

Geologic Setting

The Rio Jacaré intrusion is located in the south-central part of Bahia state in northeastern Brazil (Fig. 1) and lies within the São Francisco craton, which in this area is composed of the Contendas-Mirante supracrustal sequence and the Gavião and Jequié blocks. The intrusion is located on the eastern edge of the Contendas-Mirante sequence, which forms a large anticlinorium trending approximately north-south. The supracrustal rocks are located between the early Archean Gavião block (3.4–3.0 Ga) to the west, which is composed predominantly of tonalite-trondhjemite granodiorite, and the Archean (2.9–2.6 Ga) Jequié block to the east, which is composed predominantly of charnockite and enderbite with strong calc-alkaline affinities and granulite facies rocks (Teixeira et al., 2000). The Contendas-Mirante sequence is thought to be younger than the adjacent Gavião and Jequié blocks and consists of an Archean basal volcanic unit overlain by a Paleoproterozoic member containing flysh and metavolcanic rocks that are overlain by a clastic member. An Rb/Sr age of 2.0 Ga for granite derived from melting of the Contendas-Mirante metapelites corresponds to the timing of the Transamazonian orogeny (2.14–1.94 Ga; Teixeira et al., 2000). The Contendas-Mirante sequence was deformed by the collision of the Gavião and Jequié blocks during the Transamazonian orogeny and is now located along part of the major Contendas-Jacobina lineament (Teixeira et al., 2000).

The Rio Jacaré Intrusion

The Rio Jacaré mafic-ultramafic intrusion, composed mainly of gabbro, is a linear sheetlike structure that strikes almost north-south, with a length of approximately 70 km, an average width of 1.2 km, and a dip of 70° E. The overall dip of the layering is also approximately 70° E, and the rocks of the intrusion commonly have a foliation subparallel to the layering. The intrusion has been described previously as a sill intruded into the volcanic rocks of the lower unit of the Contendas-Mirante sequence (Brito, 1984; Galvão et al., 1986).

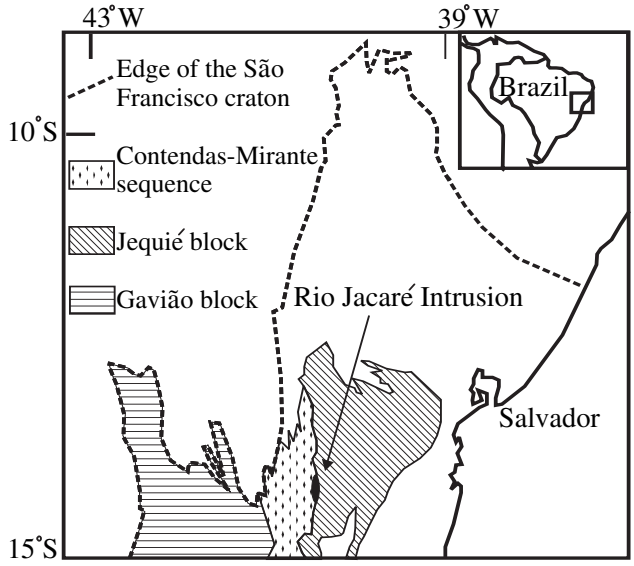

FIG. 1. Location map of the Rio Jacaré intrusion (modified from Teixeira et a., 2000).

However, the Rio Jacaré intrusion is fault bounded to the east and west, and therefore its contacts with both the Contendas-Mirante sequence and Jequié block are tectonic. The age of the intrusion is poorly known. Whole-rock dating of rocks from the intrusion itself include a Pb/Pb age of 2.47 Ga ± 72 Ma (Marinho et al., 1994), an Sm/Nd age of 2.8 Ga ± 68 Ma (Brito et al., 2001), and a zircon age of 2.64 Ga ± 5 Ma (M. M. Marinho, pers. commun.). The intrusion is cut by granite pegmatite veins that are closely related to a granite intrusion that has an age of 1.94 Ga ± 54 Ma (Marinho et al., 1994). An Rb-Sr isochron yielded an age of 1.8 Ga ± 26 Ma, corresponding to metamorphic recrystallization of the intrusion during the Transamazonian orogeny (Brito et al., 2001).

Metamorphism and deformation have modified many of the igneous textures and minerals of the intrusion. Relict minerals are rare, but some igneous textures are still preserved such as olivine cumulate textures and layering between pyroxenite and gabbro. The pyroxene in these rock types is now largely altered to hornblende, which is in turn replaced by actinolite, tremolite, and chlorite in many samples. The presence of amphibole and garnet in the gabbro and magnetitite in the Rio Jacaré intrusion indicates amphibolite-grade metamorphism.

The intrusion has been divided into an Upper and a Lower zone (Fig. 2). The Lower zone is approximately 400 m thick and consists of gabbro with some diorite and minor anorthosite. Anorthosite also occurs as a layer near the bottom of the Lower zone, has a mean thickness of 15 m, and is composed of plagioclase, with minor quartz, and chlorite that replaces pyroxene. The gabbro is massive, coarse grained, and slightly foliated, whereas the diorite is massive and mainly fine grained. The primary igneous mineralogy of the gabbro consisted of plagioclase and orthopyroxene as cumulate phases, with interstitial clinopyroxene. The orthopyroxene, clinopyroxene and olivine mineralogy has been examined in detail by Brito (2000). Quartz and biotite are present as minor phases, and apatite and titanite are common accessory phases. Within the Lower zone there are lenses of magnetite-rich rocks. The outer margins of the lenses consist of magnetite-bearing pyroxenite with 30 to 70 percent opaque minerals. The centers of the lenses consist of massive magnetitite. These bodies were previously described as forming pipes and plugs intruded into the gabbro of the Lower zone (Brito, 1984). However, the contact relationships with the gabbro are not clear because the bodies are usually bounded by faults and are poorly exposed. They are described in greater detail below.

The Upper zone has an average thickness of 600 m and is formed mainly of layered gabbro varying from leuco- to melagabbro with some cyclic units of gabbro, pyroxenite, magnetite-bearing pyroxenite, and magnetitite. The pyroxenite consists of thin layers, typically a few centimeters to less than 1 m in thickness, and which are in many cases associated with the magnetite bodies. Geochemical analyses of the pyroxenite and gabbro show fractionation with upward enrichment in Na and K from the Lower to the Upper zone and upward depletion in Ca and Mg (Table 1).

The Magnetite Bodies

The main V-rich magnetite bodies in the Rio Jacaré intrusion occur in three locations, namely Gulçari A, Gulçari B,

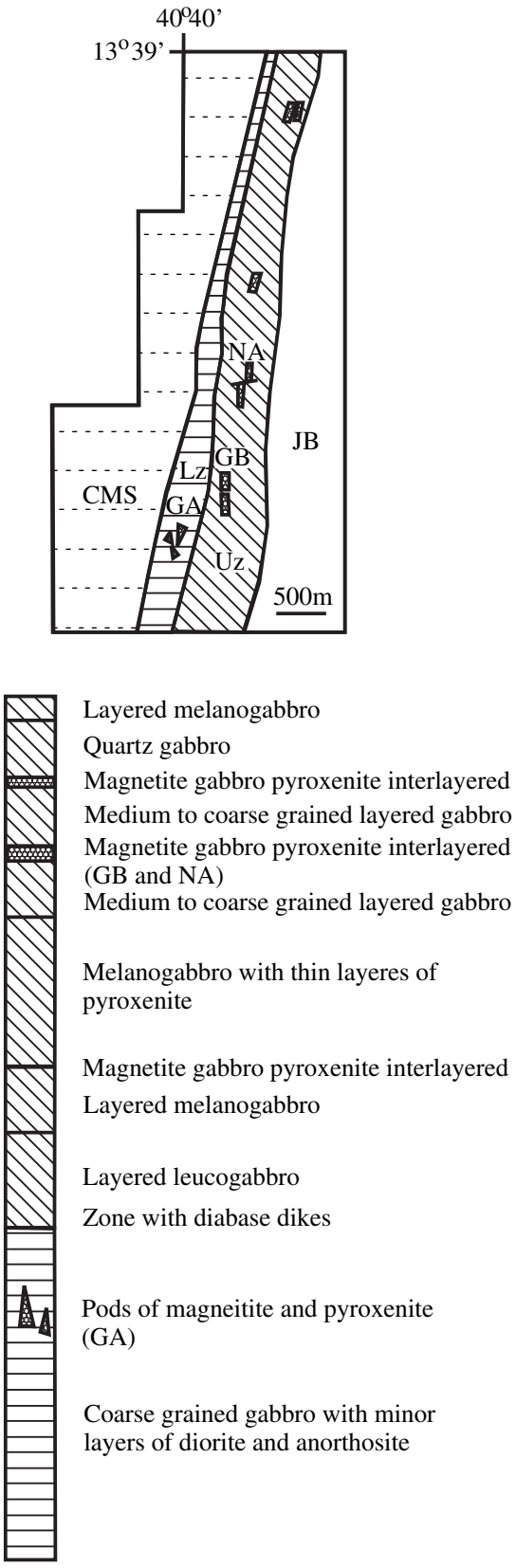

FIG. 2. Stratigraphic column and location map of the sampled magnetite bodies in the Rio Jacaré intrusion. CMS = Contendas Mirantes sequence, GA = Gulçari A, GB = Gulçari B, JB = Jequié block, Lz = Lower zone, NA = Novo Amparo, Uz = Upper zone (modified from Brito, 1984).

and Novo Amparo. Gulçari A is hosted in the gabbro of the Lower zone, whereas the other two occur in the Upper zone. The Gulçari A body contains the largest concentrations of V-rich magnetitite with estimated reserves of 80,000 t at 2.2 percent V_2O_5 and 1.6 percent TiO_2 (Brito, 1984, 2000). This body crops out over an area of approximately 350 × 100 m and has been disrupted by faulting. It is composed of magnetitite grading into magnetite-rich pyroxenite, pyroxenite, and then gabbro which contains layers or lenses of magnetite-bearing pyroxenite that are sometimes sheared (Figs. 3–4). The main magnetite body is on average 23 m thick. It has been suggested that, although the magnetite-pyroxenite body of Gulçari A is disrupted by faulting, it is a part of the main igneous sequence of the Rio Jacaré intrusion rather than a separate pipelike intrusion crosscutting the gabbro (Sá, 1992).

As in Gulçari A, the Gulçari B and Novo Amparo bodies consist of magnetitite closely associated with pyroxenite layers and hosted in gabbro (Fig. 4). The magnetitite layers have

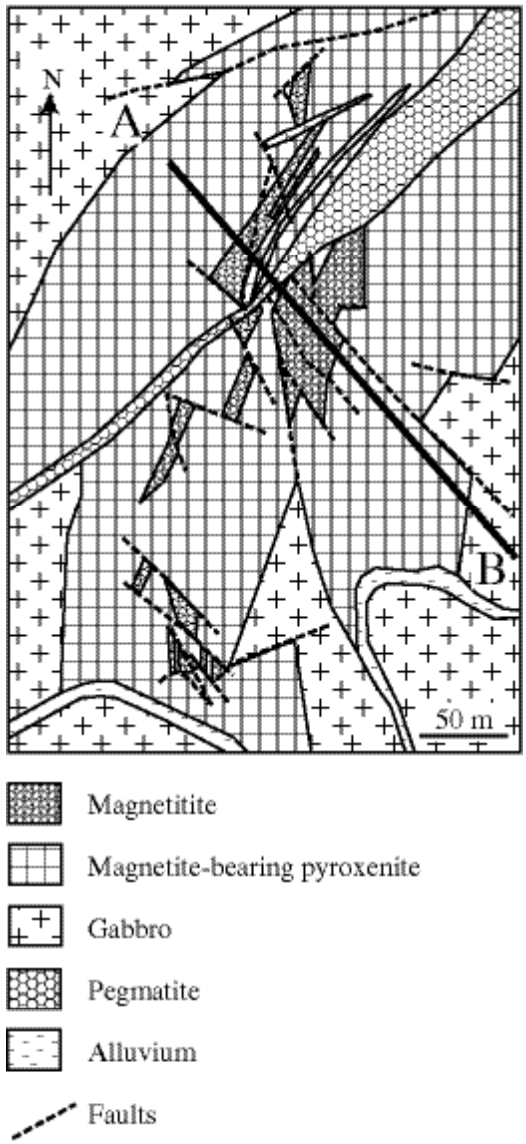

FIG. 3. Map of Gulçari A, located in Figure 2 (modified from Brito, 1984).

TABLE 1. XRF Analyses of Gabbro and Pyroxenite from the Rio Jacaré Intrusion

	1	2	3	4	5	6	7	8	9
SiO_2 (wt %)	48.7	50.0	48.1	40.8	43.6	36.3	48.4	48.0	37.7
TiO_2	1.3	1.0	1.7	3.8	4.3	4.9	1.1	2.3	4.5
Al_2O_3	14.2	15.4	14.2	14.8	14.8	2.4	5.2	13.7	14.0
FeO	17.6	15.6	18.8	25.9	24.0	31.5	21.4	19.3	26.7
MnO	0.2	0.2	0.2	0.2	0.2	0.3	0.3	0.2	0.1
MgO	5.3	5.1	5.4	4.3	3.3	10.4	11.1	4.9	5.4
CaO	8.9	9.1	9.0	6.6	6.3	12.9	11.6	8.1	9.9
Na_2O	2.7	2.6	2.5	2.8	3.1	0.5	0.8	2.5	1.6
K_2O	0.4	0.3	0.4	0.9	1.0	0.1	0.3	0.4	0.6
P_2O_5	0.1	0.1	0.1	0.1	0.1	0.0	0.1	0.1	<0.1
Total	99.4	99.4	100.4	100.2	100.7	99.3	100.3	99.5	100.5
V (ppm)	706	587	1047	176	213	3894	1281	653	958
Cr	22	22	34	1	<1	6	28	26	9
Ni	70	64	82	17	16	246	232	93	123

Notes: 1, 2, and 3 = gabbro from the Lower zone, 4 and 5 = gabbro from the Upper zone, 6 and 7 = magnetite-rich pyroxenite and pyroxenite from the Gulçari A deposit, 8 = pyroxenite associated with massive magnetite from the Gulçari B deposit, and 9 = pyroxenite associated with the massive magnetite from the Novo Amparo deposit

a width between 8 and 13 m and lengths of up to 250 m, with the layers being truncated by faults. The magnetitite layers in the Upper zone have sharp magmatic contacts with gabbro below and gradational contacts with the gabbro above.

Sampling and Analysis

Fifty-five drill core samples were selected for analysis from three drill holes: GA41, which crosscuts the Lower zone magnetite lens (Gulçari A), and GB1 and NA1 which crosscut two of the Upper zone magnetite lenses (Gulçari B and Novo Amparo).

Major and trace element concentrations in whole-rock samples were analyzed by XRF, and silicate minerals were analyzed using a JEOL electron microprobe, both at the University of Leicester. PGM and sulfides were analyzed on a Cambridge instruments S360 SEM at the University of Cardiff, using an Oxford Instruments AN10000 EDX analyzer. Operating conditions for the quantitative analyses were 20 kV, with a specimen calibration current of ~1 nA and a working distance of 25 mm. Counting times were 100 s. A cobalt reference standard was analyzed regularly and frequently, in order to check for any drift in the analytical conditions. A comprehensive set of standards, used to calibrate the EDX analyzer, was obtained from Micro Analysis Consultants Ltd. (St Ives, Cambridgeshire). ZAF corrections were

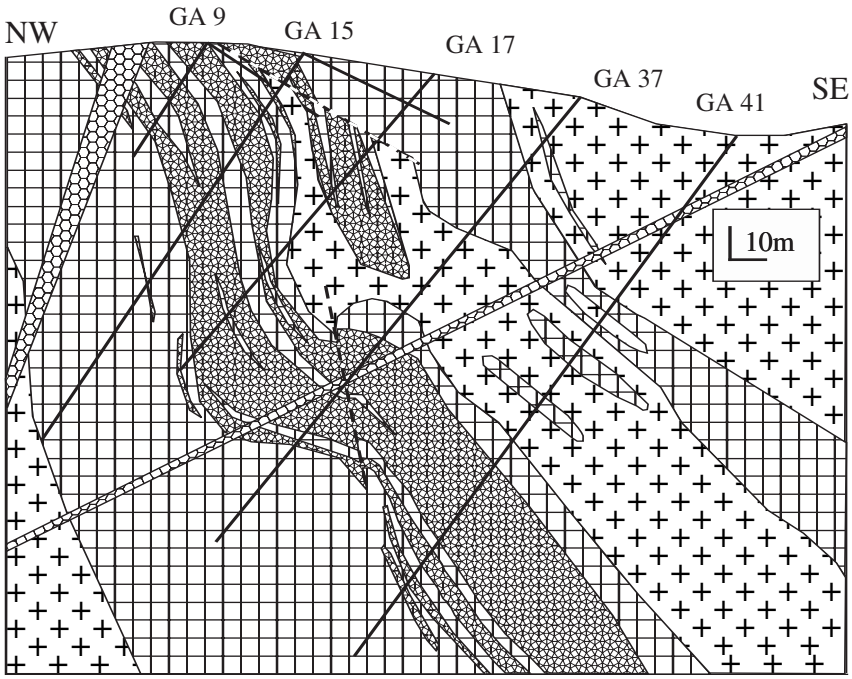

FIG. 4. Vertical cross section of Gulçari A, showing the position of drill sites GA 9, GA15, GA17, GA37, and GA41. For the legend, see Figure 3 (modified from Brito, 1984, and Galvão et al., 1986).

performed using the AN 10000 program ZAF4-FLS. The majority of the PGM were too small for quantitative analysis, and results for PGM, sulfides, and arsenides of only 1 to 2 μm in diameter are semiquantitative. Images were obtained using a four-quadrant backscattered electron detector operating at 20 kV, a beam current of ~500 pA, and a working distance of 13 mm, under which conditions magnifications up to 15,000 × were possible.

Sulfur, Cu, and Ni were determined at McGill University; S by LECO titration, Ni by X-ray fluorescence, and Cu by atomic absorption analysis. The PGE analyses were carried out at the University of Quebec, Chicoutimi. The PGE were collected from 50 g of sample by a 26-g NiS bead using the method of Robert et al. (1971). The beads were dissolved in HCl, which dissolved the Ni, S, and most chalcophile elements, leaving a residue of precious metals. These were then collected on millipore filter paper. The precious metal residue and filter papers were irradiated at Ecole Polytechinique, Montreal, with a neutron flux of $5 \times 10^{15}\ m^{-2}s^{-1}$. The first irradiation was for 3 min, after which the gamma-ray spectra for Rh were collected. The samples were then irradiated for a further 4 h. The spectra for Pd were collected between 20 and 30 h after irradiation. Both the Rh and Pd spectra were collected using a planar detector. The spectra for the remaining PGE and Au were collected between 5 and 7 days after irradiation, using a semiplanar detector. The accuracy and precision for results obtained at the University of Quebec, Chicoutimi, were estimated from five determinations of the international standards UTM-1 and WGB-1 (Table 2). A blank sample consisting of 20 g of silica also was analyzed, giving blank values of 0.02 ppb Ir and 0.3 ppb Au.

Mineralogy

Oxides

Magnetite is the major oxide phase in the magnetitite, followed by ilmenite. The magnetite normally occurs as anhedral grains, with grain sizes of between 0.3 and 2.0 mm and forms a polygonal mosaic together with ilmenite. Ilmenite also occurs as inclusions in the magnetite, commonly displaying exsolution textures. Silicate phases associated with the magnetite include plagioclase, hornblende, and rare grains of clinopyroxene and olivine. Magnetite from the magnetitite in the lower (Gulçari A) body has higher V_2O_5 concentrations (2.2–4.5 wt %) than magnetite from the Upper zone (Gulçari B and Novo Amparo, 0.3–2.5 wt % V_2O_5; Brito, 2000).

Silicates

Rare olivine and pyroxene grains were observed within the magnetitite but most are altered to serpentine or chlorite. Microprobe analyses of these grains (Table 3) show that olivine in the magnetitite ranges in composition from Fo_{49} to Fo_{61}, and the clinopyroxene is diopside with compositions in the range of En_{82} to En_{87}. The Rio Jacaré intrusion has been intensely metamorphosed and so the pyroxene compositions observed probably reflect metamorphic reequilibration rather than original magmatic compositions. In addition, Brito (2000) also documented the presence of orthopyroxene. Garnet and biotite are present in the Gulçari B and Novo Amparo bodies.

Sulfides and arsenides

Sulfides account for up to 1 vol percent of the rock in the magnetitite. The major phases are chalcopyrite and pentlandite with only very minor pyrite and pyrrhotite. Chalcopyrite is much more abundant than the other sulfides and is most common in the rock types containing 50 vol percent magnetite or less. It commonly occurs interstitially to magnetite or ilmenite enclosed by amphibole and plagioclase. Pentlandite is much less abundant and occurs in the magnetitite. The pentlandite tends to occur interstitially to the magnetite and ilmenite in silicates but, locally, composite grains of pyrrhotite, pentlandite, and chalcopyrite are enclosed in magnetite. A few sphalerite and galena grains were found together in the silicates, associated with the other sulfides especially in the magnetite-poor rock types. However, the dominant trace minerals smaller than 50 μm are Ni and Co sulfarsenides and arsenides and Co rich pentlandite. Representative analyses are given in Table 4. The arsenides are typically very inhomogeneous, and it was only possible to analyze them qualitatively. In many cases the arsenides are associated with the sulfides and appear to be alteration products of the sulfides. The base metal-rich sulfides are accompanied by rare Au-Ag and Au-Cu alloys, native Au and Cu, Bi and Re sulfides, and in one sample 14 grains of Ag sulfide were qualitatively identified.

TABLE 2. Precision and Accuracy of PGE Analyses Based on the Results for Canadian Certified Reference Materials

	UTM[1]				WGB-1			
	(ppb)	± (ppb)	UQAC[2] (ppb)	±[3] (ppb)	(ppb)	± (ppb)	UQAC (ppb)	± (ppb)
Os	*8*		7.58	1	(0.5)		<0.5	
Ir	8.8	0.6	8.59	0.5	(0.33)		0.21	0.04
Ru	11	1.5	12.7	2.5	(0.3)		<5	
Rh	9.5	1.1	10.3	0.5	(0.32)		0.4	0.16
Pt	129	5	133	9	6.1	2.6	4	1.2
Pd	106	3	95.4	5	14	2.1	11	3
Au	48	2	51.6	2.5	2.9	1.1	1.5	0.04

[1]Certified values and errors issued by Canada Centre for Mineral and Energy Technology (CANMET) for the reference materials UMT-1 and WGB-1, values in parentheses are approximate

[2]Average of values obtained at Université du Quebec a Chicoutimi (UQAC)for five different NiS beads

[3]The standard deviations for five different NiS beads

TABLE 3. Microprobe Analyses of Olivine (col. 1–3) and Pyroxene (col. 4–7) from Magnetite in the Gulçari A Deposit

SiO_2	34.5	35.9	34.7	52.7	53.2	52.9	53.2
TiO_2	<0.1	<0.1	<0.1	<0.1	0.1	0.1	0.1
Al_2O_3	<0.1	<0.1	<0.1	0.4	0.6	0.4	0.7
FeO	42.1	33.8	38.2	4.8	4.3	6.0	4.6
MnO	0.6	0.5	0.7	0.1	0.1	0.2	0.2
MgO	22.9	30.6	26.9	16.2	16.4	15.4	16.3
CaO	<0.1	<0.1	<0.1	25.7	25.2	25.1	24.9
Total	100.1	100.8	100.5	99.9	99.9	100.1	100.0
Mg no.	49.2	61.7	55.6	85.8	87.2	82.1	86.3

TABLE 4. Representative Microprobe Analyses of Sulfide Minerals

Mineral	1	2	3	4	5	6	7
Fe (wt %)	30.9	46.98	60.34	28.94	24.58	13.77	8.50
Co	-	-	-	7.08	9.41	15.24	-
Ni	-	-	-	30.09	32.66	28.61	-
Cu	34.00	-	-	-	-	-	-
Zn	-	-	-	-	-	-	58.15
S	34.89	52.68	37.82	32.68	32.47	41.63	34.06
Total	99.00	99.66	98.16	98.80	99.13	99.25	100.71

Notes: 1 = chalcopyrite $CuFeS_2$, 2 = pyrite FeS_2, 3 = pyrrhotite FeS, 4 and 5 = Co pentlandite $(Ni,Fe,Co)_{9.0}S_8$ and $(Ni,Fe,Co)_{9.1}S_8$, 6 = linnaeite $(Ni_6,Fe_3,Co_3)S_{16}$, 7 = sphalerite $(Zn,Fe)_{0.98}S_1$; - = below detection limit

Platinum-group minerals

More than 100 PGM grains have been identified qualitatively in a total of eight polished thin sections of magnetitite and magnetite-bearing pyroxenite from the samples with the highest PGE concentrations. Most PGM are less than 5 μm in diameter but 14 grains have diameters between 5 and 10 μm. The PGM are Pd and Pt minerals with minor Rh. The most common Pd minerals are Pd antimonides (17 grains), Pd bismuth-antimonides (21 grains), Pd bismuth tellurides (8 grains), and Pd bismuthides (4 grains). Sperrylite is the most abundant Pt mineral (25 grains, 6 with a maximum diameter of between 5 and 10 μm). Two Pt antimonide grains, with diameters of between 5 and 10 μm, were located in one sample. Other As-rich PGM include Pd-Ni arsenides and hollingworthite (RhAsS). All the remaining PGM are Pd or Pt alloys. Pd combines with Cu, Sn, and Au to form Pd-Cu-Sn alloys (6 grains) and minor Au-Cu-Pd (4 grains), whereas Pt combines with precious and base metals to form Pt-Cu (probably hongshiite PtCu), Pt-Au, Pt-Fe, and one grain of Pt-Ni.

The Pd and Bi antimonides, Pd bismuthide tellurides, and Pd alloys are irregular or subrounded and in many cases form composite grains with two or three PGM containing the same PGE (e.g., Pd antimonides with Pd tellurides and Pd bismuthides). The Pd minerals are typically associated with magnetite or ilmenite and are mainly located adjacent to silicate inclusions or at grain boundaries between magnetite and ilmenite or silicate. In many cases the Pd minerals are associated with Co-rich pentlandite and in a few samples with inhomogeneous Co and Ni arsenides. Pd antimonide blebs occur within Co arsenides and sulfarsenides, which appear to have formed from alteration of pentlandite (Fig. 5A). Pd antimonides tend to be enclosed in magnetite or ilmenite but are associated with silicate inclusions and in some cases spinel (Fig. 5B), whereas Pd bismuthides and tellurides tend to occur at the edges of magnetite and ilmenite grains in contact with silicates. Rarely, Pd minerals are aligned along fractures suggesting that some remobilization has occurred (Fig. 5C). Two grains of Pb-Pd alloys were observed in magnetitite; one enclosed by magnetite and the other by silicate. Pd minerals large enough to be analyzed are taimyrite $Pd_9Cu_3Sn_4$ (analyses 1–2, Table 5; Cabri, 2002) and froodite $(Pd,Sn,Cu)Bi_2$ (analysis 3, Table 5), similar to that described from Sudbury by Cabri and Laflamme (1976).

Sperrylite tends to occur in more silicate- and less magnetite- and ilmenite-rich parts of samples. It usually forms euhedral crystals but it may have subrounded outlines. In many cases sperrylite is enclosed by silicate and, in a few cases, by ilmenite or magnetite or it occurs at contacts between these minerals. In one case, sperrylite is enclosed in a rounded silicate-filled inclusion in magnetite (Fig. 5D) and in another case enclosed in olivine (Fig. 5E-F). Sperrylite is commonly associated with Co or Ni arsenides and rarely with hollingworthite. In several cases, well-formed sperrylite crystals occur adjacent to irregular Pt-Fe alloys, both in silicates and enclosed by magnetite. In one case, a sperrylite grain at the contact with an olivine and an amphibole grain is altered to an irregular Pt-Fe alloy where it is in contact with the amphibole grain (Fig. 5F). A Pt-Ni alloy enclosed in amphibole and located at the contact of magnetite and olivine (Fig. 5E) may also be an alteration product of a PGM. One Pt-Fe alloy is enclosed in magnetite and appears not to have altered from sperrylite.

Of the sperrylite grains that were large enough to be analyzed quantitatively, all have a very similar composition. Three typical analyses are given in Table 5 (analyses 8–10). The analyzed sperrylite contains 2 to 3 percent Fe, and the grains are large enough that this is unlikely to be a contribution of Fe from the minerals surrounding them. Polished sections of magnetitite were analyzed before and after immersion in dilute hydrochloric acid, which should dissolve any Fe contamination from polishing of the host magnetite. The sperrylite grains in these samples were found to contain Fe both before and after the acid treatment. Similar sperrylite from other occurrences in ophiolites (Prichard and Tarkian, 1988) that were analyzed at the same time were free of Fe. These observations confirm that Fe in the sperrylite from the Rio Jacaré intrusion is not an artifact of sample preparation or of analysis. The Fe is observed to be homogeneous throughout the sperrylite grains with no decrease from the edges toward the centers of the larger grains. If Fe is ignored in the calculation of the formula then the sperrylite is perfectly stoichiometric. Fe is not normally present in sperrylite, which is usually pure $PtAs_2$ with no trace elements (Cabri and Laflamme, 1976). Although up to 1.5 wt percent Fe has been recorded in sperrylite from the Witwatersrand reefs in South Africa (Feather, 1976), these samples show complicated intergrowth textures with their host silicates. The Fe in the sperrylite in the Rio Jacaré intrusion may be a result of the very Fe rich composition of the magma that formed the magnetite and Fe-rich olivine which hosts the sperrylite.

The sheared magnetite-bearing pyroxenite in gabbro from Gulcari A (Fig. 4, Table 6) contains isolated high concentrations

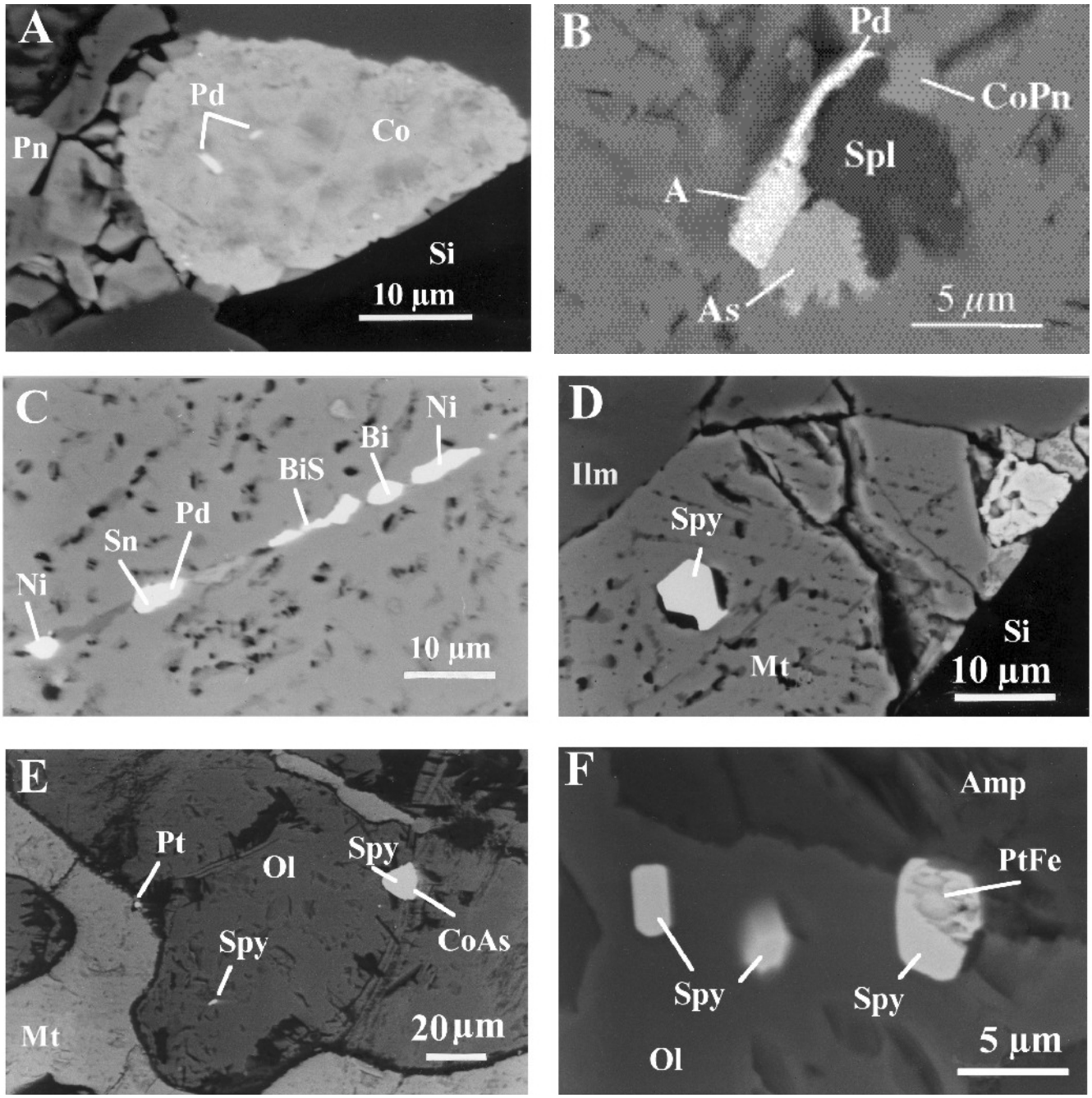

FIG. 5. Backscattered electron images of PGM. A. A subrounded mottled inhomogeneous Co sulfarsenide grain (Co), containing two elongate grains of Pd antimonide (Pd). The arsenide is adjacent to a pentlandite grain (Pn) and silicate (Si). B. A cluster of PGM enclosed within magnetite (Mt). A composite PGM is composed of a thin lath of Pd antimonide (Pd) and a subrounded more equigranular grain (A) of a Pd-bearing Cu-Au alloy (analysis 4, Table 5) that is adjacent to a Ni arsenide (As). A Co-bearing pentlandite (CoPn) is also present. The PGM are associated with an Fe-, Al-, and Mg-bearing spinel (Spl). C. A row of five Pd-bearing sulfides and bismuthides crossing a magnetite grain. From left to right these inclusions are a rounded Ni-Bi arsenide (Ni), a composite grain (Sn) of $(Pd,Cu)_3Sn$ (analysis 1, Table 5), and a Pd bismuthide (Pd), an elongate Bi sulfide (BiS), a rounded (Bi)-Pd bismuthide (analysis 3, Table 5), and another elongate Ni-Bi arsenide. D. A euhedral sperrylite grain (8-μm diam; Spy) contained in a silicate inclusion (Si) enclosed by magnetite (Mt) at the edge of an ilmenite (Ilm) grain. E. A PGM in olivine (Ol) adjacent to magnetite (Mt). The largest PGM shown is a sperrylite (Spy), which is cut by a secondary vein where it is replaced by an Ni-Co-Fe arsenide (CoAs). A smaller elongate sperrylite (Spy) is enclosed by olivine. A third small PGM, a Pt-Ni alloy (Pt), is located at the contact of the olivine and the magnetite. It is suggested that the Pt-Ni alloy is an alteration product as it is situated within fibrous amphibole. F. Three sperrylite grains (Spy) within silicate. The grain on the left corresponds to analysis 9, and the grain in the center corresponds to analysis 10 (Table 5). The sperrylites lie almost entirely within olivine (Ol) except for the largest grain (5-μm diam), which has its upper part at the contact of the olivine with an amphibole grain. Where the PGM is in contact with the amphibole (Amp) it forms a Pt-Fe alloy (PtFe), which appears to be an alteration product of sperrylite.

TABLE 5. Microprobe Analyses of Platinum-Group Minerals

Mineral	1	2	3	4	5	6	7	8	9	10
Rh (wt %)	-	-	-	-	0.6	-	-	0.6	-	0.6
Pd	52.2	48.4	25.8	9.3	-	-	0.9	-	-	-
Pt	-	5.0	-	-	47.4	68.7	34.1	54.8	53.8	53.2
Au	-	-	-	40.1	-	-	7.7	-	-	-
Sn	28.3	27.9	1.2	-	-	-	3.7	-	-	-
Ti	-	-	-	-	1.0	5.2	-	(0.4)	-	-
V	-	-	(0.3)	-	-	-	-	-	-	-
Co	-	(0.8)	-	-	-	-	0.5	-	-	-
Fe	(3.7)	(1.4)	(4.5)	6.0	21.7	23.6	4.7	(1.8)	(3.4)	(3.0)
Ni	-	(1.3)	0.6	1.0	27.0	1.2	0.7	(0.3)	-	-
Cu	14.6	14.6	3.2	42.3	0.6	0.7	47.9	-	-	-
As	-	-	-	-	-	-	-	41.8	41.1	42.4
Bi	-	-	64.5	-	-	-	-	-	-	-
Sb	-	-	-	-	-	-	-	-	-	0.5
Total	99.8	99.4	100.1	98.7	98.3	99.4	100.2	100.3	98.3	99.7

	Formula	Size in μm	Mineral associations
1. Taimyrite	$(Pd_{8.19}Cu_{0.81})_9Cu_{3.02}Sn_{3.98}$	3 × 3	In magnetite
2. Taimyrite	$(Pd_{7.70}Cu_{0.89}Pt_{0.43})_{9.02}Cu_{3.00}Sn_{3.98}$	5 × 5	With Fe-Co-Ni sulfide and spinel
3. Froodite	$(Pd,Sn,Cu,Ni)_{0.97}Bi_{2.03}$	3.5 × 2	In magnetite
4. Alloy	$Cu_{0.62}Au_{0.19}Fe_{0.10}Pd_{0.08}Ni_{0.01}$	3 × 1.7	Magnetite, Ni arsenide and spinel
5. Alloy	$Pt_{0.21}Fe_{0.35}Ni_{0.41}Ti_{0.02}Cu_{0.01}$	2 × 2	In silicate
6. Alloy	$Pt_{0.39}Fe_{0.46}Ni_{0.02}Ti_{0.12}Cu_{0.01}$	3 × 2	In ilmenite
7. Alloy	$Pt_{0.16}Cu_{0.67}Fe_{0.07}Au_{0.04}Sn_{0.03}Ni_{0.01}Pd_{0.01}Co_{0.01}$	9 × 3	With Fe-Co-Ni sulfide and magnetite
8. Sperrylite	$(Pt_{0.99}Rh_{0.02})_{2.01}(As_{1.97}Sb_{0.02})_{1.99}$	10 × 10	With ilmenite and magnetite
9. Sperrylite	$Pt_{1.00}As_{2.00}$	2 × 2	In silicate
10. Sperrylite	$(Pt_{0.97}Rh_{0.02})_{0.99}(As_{2.00}Sb_{0.01})_{2.01}$	5.7 × 4	In silicate

Concentrations of elements shown in brackets have not been used in the calculation of the platinum-group mineral formulas

of Pt and Pd (samples GA41 at a 55-m depth and GA41 at a 56-m depth). Samples of the PGE-enriched material were examined for PGM and the assemblage was found to be similar to that in the nonsheared rocks. This includes sperrylite that occurs as 2- to 10-μm grains enclosed in magnetite or at the contact between magnetite and ilmenite or magnetite and silicates. Pd antimonides, bismuthides, tellurides, and Pd-Ni antimonides occur as 2- to 3-μm-sized minerals, commonly grouped together to form composite PGM within ilmenite. Pt and Pd PGM occur together in the composite grains. These PGM are accompanied by Co-rich pentlandite and Co-Ni arsenide.

Geochemistry

The metal and sulfur contents of the magnetite bodies and their host lithologies vary by two to three orders of magnitude (Table 6). The Cu and S concentrations range from 10 to 6,000 ppm, Ni values have a smaller range from 10 to 700 ppm, and gold concentrations range up to 315 ppb (Table 6, Figs. 6–7). Platinum concentrations are typically slightly higher than Pd, with an average Pt/Pd ratio of 1/4. In most rocks these elements occur at concentrations in the 10- to 500-ppb range. However, sample GA41 at a 55-m depth is enriched in Pt and all other PGE except Pd, and sample GA41 at a 56-m depth is enriched in Pd. In all samples Ir and Rh concentrations are very low (0.03–10 ppb) but most samples contain 0.1 to 1 ppb (Table 6, Figs. 8–9).

The magnetite-bearing rocks (magnetitite and magnetite-bearing pyroxenite) from each unit contain more metals than the host gabbro (Table 7). The Upper zone magnetite-bearing rocks (Gulçari B and Novo Amparo) are also richer in sulfur than the host silicate rocks. The Lower zone silicate rocks (Gulçari A) are slightly richer in sulfur than the magnetitite, but the difference is not significant. The average concentrations of Ni and all of the PGE, except Pd, are similar for all three magnetite lenses (Table 7). However, the average Cu and S values are higher in the Upper zone magnetite lenses (Gulçari B and Novo Amparo), and the average Pd is lower than in the Lower zone (Table 7). Gold concentrations are similar in the Lower zone magnetite-bearing rocks at Gulcari A and in the Upper zone magnetite-bearing rocks at Novo Amparo, but the Gulçari B lens has lower Au values. Lower zone samples have higher Ni/Cu and higher Pd/Ir ratios.

Within each lens the metals show similar behavior. In the Upper zone lens of Novo Amparo the concentrations of metals and sulfur are positively correlated (Fig. 6A). In detail, PGE and Ni concentrations closely follow each other, as do Cu, Au, and S (Fig. 6A). Trends for Cu, Au, and S are generally similar to the trends for Ni and the PGE, but at 55, 36.5, and 30.3 m concentrations of the PGE are low, whereas Cu and S concentrations are high. In the upper magnetitite the PGE values generally increase upsection by an order of magnitude. The base metals, Au and S, also increase but only by a factor of 1.5 to 3 (Table 6).

In the Upper zone lens (Gulçari B) concentrations of the metals and sulfur are low in the silicate rocks on either side of the lens and high in the magnetite lens. The variations in Ni and PGE concentrations correspond closely, and Cu, S, and

TABLE 6. Whole-Rock Concentrations of Ni, Cu, S, PGE, and Au from the Rio Jacaré Intrusion

Drill hole	Depth (m)	Rock type	Ni (ppm)	Cu (ppm)	S (ppm)	Ir (ppb)	Rh (ppb)	Pt (ppb)	Pd (ppb)	Au (ppb)	Pt/Pd	Pd/Ir	Cu/Pd_{mn}
GA41	23.2	Gabbro	177	106	893	0.20	0.50	18	11	1.0	1.6	55	1.34
GA41	38.4	Gabbro	72	221	3080	0.09	0.30	19	12	6.8	1.6	133	2.57
GA41	50.7	Mag.- pyx	322	59	448	0.30	0.69	33	10	0.3	3.2	34	0.80
GA41	55.0	Mag.- pyx	480	37	224	9.60	11.18	1663	47	2.0	35.2	5	0.11
GA41	56.0	Mag.- pyx	323	114	895	1.40	4.00	362	622	10.8	0.6	444	0.03
GA41	57.0	Melagabbro	187	105	225	0.07	0.31	50	143	1.9	0.4	2046	0.10
GA41	59.0	Melagabbro	138	53	300	0.09	0.23	88	77	9.9	1.1	855	0.10
GA41	61.8	Melagabbro	137	417	883	0.18	0.84	215	308	20.5	0.7	1713	0.19
GA41	65.0	Melagabbro	110	166	518	0.55	0.50	80	8	9.7	10.0	15	2.89
GA41	67.3	Mag.-pyx	195	185	550	1.80	1.90	154	30	15.1	5.1	17	0.86
GA41	68.6	Mag.-pyx	234	227	600	2.10	4.50	358	59	8.7	6.1	28	0.54
GA41	72.0	Mag.-pyx	217	74	370	1.40	1.20	212	45	3.7	4.8	32	0.23
GA41	86.0	Mag.-pyx	267	1385	1492	0.20	1.00	22	23	53.7	1.0	115	8.39
GA41	98.4	Mag.-pyx	270	1196	1641	1.20	3.00	295	212	33.2	1.4	177	0.79
GA41	100.4	Magnetitite	418	2464	1802	0.25	0.50	84	69	99.0	1.2	276	4.97
GA41	103.3	Magnetitite	409	58	522	0.80	2.00	179	188	47.3	1.0	235	0.04
GA41	107.3	Magnetitite	467	14	454	1.15	2.50	243	177	8.3	1.4	154	0.01
GA41	110.0	Magnetitite	475	32	224	1.10	2.00	250	134	25.4	1.9	122	0.03
GA41	111.8	Magnetitite	465	18	300	1.00	2.50	253	233	32.8	1.1	233	0.01
GA41	114.9	Magnetitite	492	159	296	0.90	2.50	232	297	46.0	0.8	330	0.07
GA41	118.5	Magnetitite	542	984	746	0.75	1.50	273	228	315.0	1.2	304	0.60
GA41	122.0	Magnetitite	556	145	147	0.40	0.50	213	324	11.8	0.7	810	0.06
GA41	124.6	Mag.-pyx	701	18	74	1.10	5.00	193	109	9.3	1.8	99	0.02
GA41	130.8	Mag.-pyx	249	46	149	0.15	0.84	40	39	3.4	1.0	260	0.16
GA41	134.8	Mag.-pyx	217	23	450	0.22	0.80	15	31	1.7	0.5	143	0.10
GA41	141.0	Mag.-pyx	308	104	810	0.15	0.50	74	162	26.1	0.5	1080	0.09
GA41	150.0	Mag.-pyx	199	45	526	0.08	0.39	23	26	2.5	0.9	326	0.24
GA41	169.5	Mag.-pyx	370	17	150	0.85	2.50	82	91	15.2	0.9	107	0.03
GB1	18.0	Gabbro	10	71	373	0.06	0.21	4	6	0.6	0.6	102	1.62
GB1	25.0	Magnetitite.	295	575	3640	1.10	2.00	185	61	12.4	3.0	55	1.31
GB1	26.8	Mag.-pyx.	98	24	448	0.13	0.57	146	29	2.6	5.0	226	0.11
GB1	30.3	Magnetitite	343	857	6640	0.60	3.39	124	107	10.0	1.2	178	1.12
GB1	32.0	Magnetitite	380	265	1482	1.30	6.50	196	119	5.1	1.6	92	0.31
GB1	33.4	Magnetitite	358	870	3040	0.55	2.50	92	65	8.2	1.4	118	1.86
GB1	39	Gabbro	12	796	1276	0.03	0.1	2	2	0.7	1.0	73	50.63
GB1	42.8	Gabbro	13	771	901	<0.03	<0.1	1	1	0.1	1.0	>33	107.39
NA1	22.5	Magnetitite	493	2591	1790	2.60	13.00	494	329	53.0	1.5	127	1.10
NA1	23.9	Magnetitite	458	1941	2040	1.70	7.00	205	121	33.0	1.7	71	2.23
NA1	26.1	Magnetitite	249	240	518	1.20	4.00	53	41	8.6	1.3	34	0.82
NA1	27.1	Magnetitite	427	330	2400	3.80	14.00	584	279	10.6	2.1	73	0.16
NA1	29.1	Magnetitite	463	500	2720	2.50	8.00	447	359	22.9	1.2	144	0.19
NA1	30.3	Magnetitite	268	1053	1351	0.10	0.50	16	12	18.0	1.3	120	12.22
NA1	31.1	Magnetitite	389	557	1193	0.30	1.74	76	34	4.9	2.2	113	2.28
NA1	35.7	Magnetitite	253	200	444	0.30	1.00	52	42	2.5	1.2	140	0.66
NA1	36.7	Magnetitite	199	999	1285	0.10	0.50	15	12	16.8	1.3	120	11.60
NA1	38.5	Mag.-pyx.	120	22	74	0.05	1.00	2	5	0.5	0.4	100	0.61
NA1	39.4	Magnetitite	351	2431	2120	0.10	0.20	30	26	50.5	1.2	260	13.02
NA1	40.3	Magnetitite	446	6282	5880	0.20	1.00	41	32	87.0	1.3	160	27.34
NA1	41.5	Magnetitite	297	3134	3200	0.05	0.50	28	18	52.4	1.6	360	24.25
NA1	42.7	Magnetitite	354	1334	1715	0.10	0.70	24	11	19.0	2.2	110	16.89
NA1	44.6	Magnetitite	245	1817	1576	0.15	1.00	34	30	23.0	1.1	200	8.44
NA1	45.6	Magnetitite	252	1510	1417	0.05	0.50	12	10	20.6	1.2	200	21.03
NA1	46.9	Mag.-pyx.	144	195	151	0.15	0.20	10	8	2.7	1.3	53	3.40
NA1	55.0	Gabbro	10	780	963	0.05	0.20	4	2	0.4	2.0	40	54.32

Notes: Also determined but not detected were Os <2 ppb and Ru <5 ppb, except in sample GA 41 at a 55-m depth, which contained 8 ppb Os; Mag- pyx = magnetite-bearing pyroxenite, mn = mantle normalized

Au also mimic each other. However the highest concentrations of Cu, Au, and S occur at 30.3 m, and the highest concentrations of PGE and Ni occur at 32 m (Fig. 6B).

In the Lower zone lens (Gulçari A), Ni and the PGE also show very similar trends (Fig. 7). Iridium and Rh and Pt and Pd are strongly correlated with each other, but Pt and Pd are highest at 146 m and Ir and Rh are highest at 124.6 m (Fig. 7). As was observed in the Upper zone, Cu, S, and Au are positively correlated but with the highest concentrations at different depths than those of Ni and the PGE (e.g., 118, 100.4, 86, and 38 m, Fig. 7). The Cu concentrations are lower in the magnetitite than in the magnetite-bearing pyroxenite, which contrasts with the other chalcophile elements.

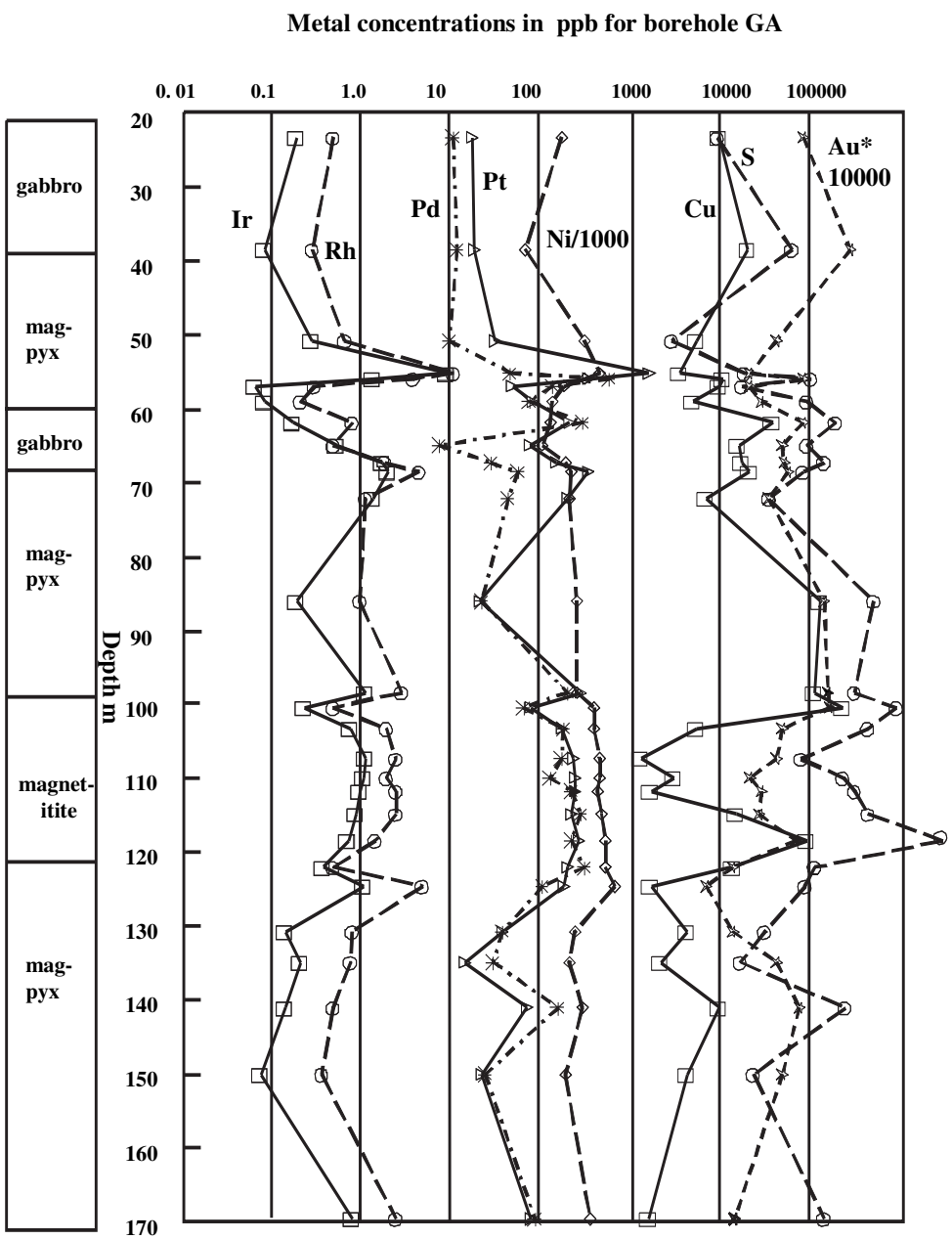

FIG. 6. S, Cu, Au, Ni, Pt, Pd, Rh, and Ir concentrations vs. depth for bore hole NA1 through the Novo Amparo magnetite body and bore hole GB1 through the Gulçari B magnetite body.

TABLE 7. Average Concentrations of Metals and Sulfur Concentration in Rocks from Rio Jacaré

Drill hole	*n*	Ni (ppm)	Cu (ppm)	S (ppm)	Ir (ppb)	Rh (ppb)	Pt (ppb)	Pd (ppb)	Au (ppb)	Pd/Ir	Pt/Pd
Magnetitites and magnetite-bearing pyroxenite											
GA	21	366	351	602	0.82	1.92	171	148	36.6	254	1.75
NA	17	318	1479	1757	0.79	3.23	125	81	25.1	140	1.41
GB	5	295	518	3050	0.74	2.99	149	76	7.8	134	2.45
Gabbros											
GA	6	137	178	983	0.20	0.45	78	93	8.3	803	2.57
NA	1	10	780	963	0.05	0.20	4	2	0.4	40	2
GB	3	12	546	850	0.04	0.14	2	3	0.5	69	0.85

Abbreviations: GA = Gulçari A, GC = Gulçari B, NA = Novo Amparo, *n* = number of samples

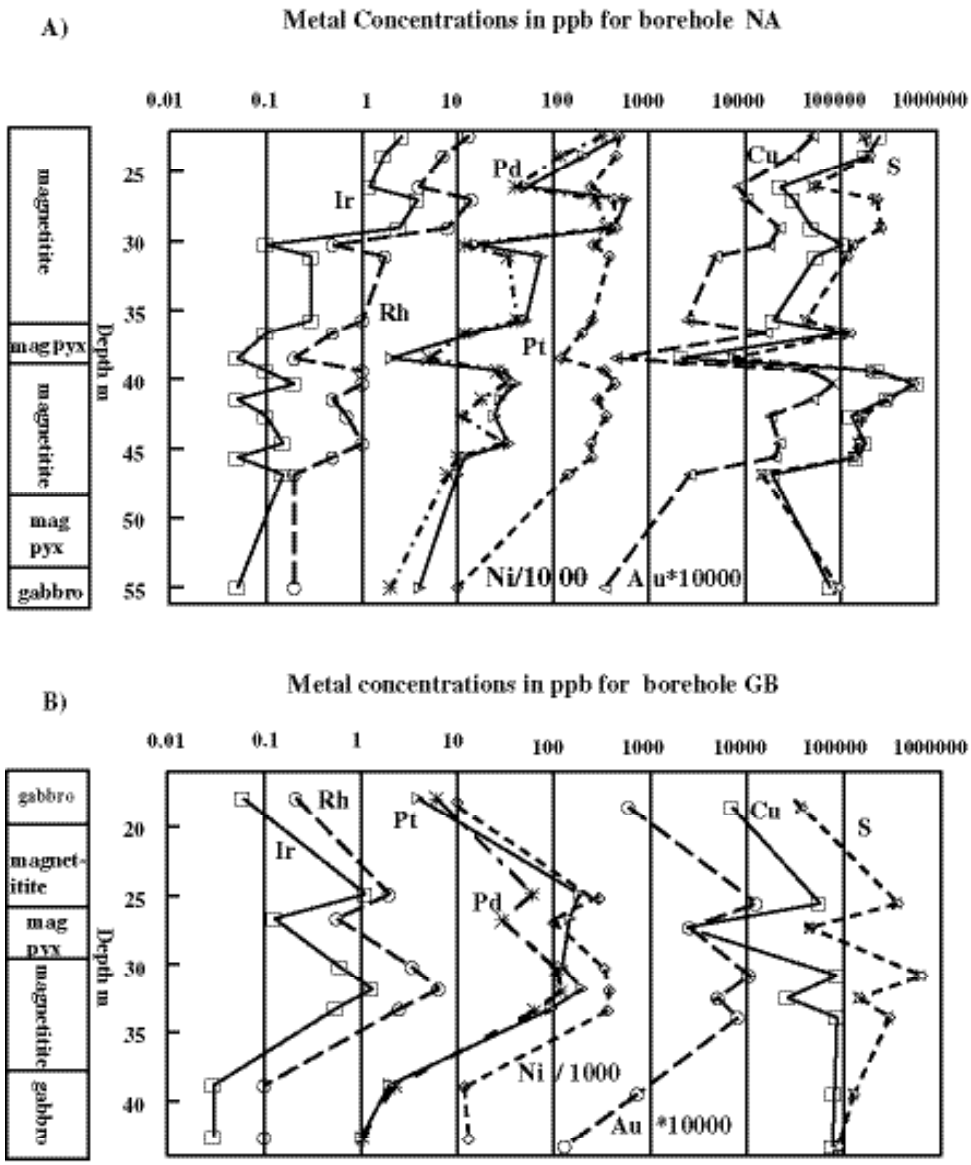

FIG. 7. S, Cu, Au, Ni, Pt, Pd, Rh, and Ir concentrations vs. depth for bore hole GA41 through the Gulçari A magnetite body.

Mantle-normalized metal patterns

Inspection of the mantle-normalized metal concentrations from the magnetite-bearing rocks (both the magnetitite and magnetite-bearing pyroxenite) reveals three different patterns. Samples with mantle-normalized (mn) ratios Cu/Pd_{mn} greater than 2 are referred to here as depleted in PGE, those with Cu/Pd_{mn} ratios of 0.5 to 2 are referred to as undepleted, and those with Cu/Pd_{mn} ratios less than 0.5 are considered enriched in PGE (Table 8).

The depleted samples are mostly from the Upper zone lens (Novo Amparo) and have Ni concentrations that are 0.1 to 0.2 times mantle and Ir concentrations that are 0.01 to 0.08 times mantle (Fig. 8). From Ir to Cu the concentrations increase steadily to Cu concentrations that are 40 to 200 times mantle. The samples with undepleted patterns are found in all three zones. These patterns begin at 0.1 to 0.2 times mantle for Ni and rise to 6 to 100 times mantle for Pt. From Pt to Cu the patterns are flat, although both positive and negative Au peaks are present. The PGE-enriched samples are mainly from the Lower zone. Nickel varies from 0.1 to 0.5 times mantle, Ir varies from 0.01 to 0.5 times mantle, and from Ir to Pd the patterns increase steadily. Palladium varies from 1 to 100 times mantle, but concentrations decrease from Pd to Cu. The undepleted samples and PGE-enriched samples have similar PGE concentrations, but the PGE-enriched samples contain less Cu and Au than the undepleted samples (Table 8).

The melagabbro and gabbro of the Lower zone (Gulçari A) have mantle-normalized metal patterns between Pt and Cu that resemble the PGE-enriched magnetite-bearing rocks (Fig. 8D). However, the Ir and Rh contents are an order of magnitude lower, resulting in much steeper patterns than for any of the magnetite-bearing rocks (Pd/Ir = 800). The patterns

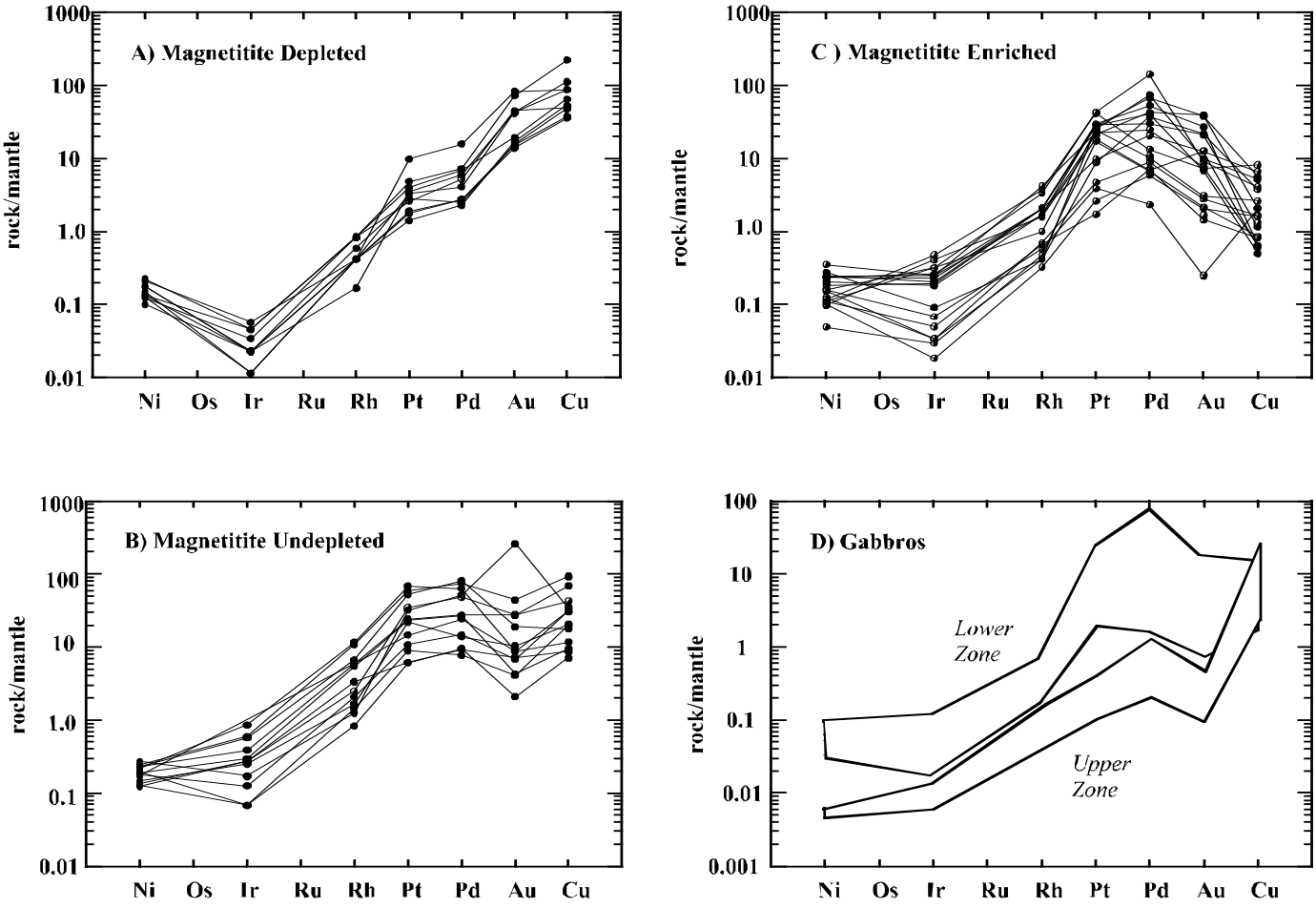

FIG. 8. Mantle-normalized rock values of Ni, PGE, Au, and Cu for (A) depleted magnetitite, (B) undepleted magnetitite, (C) enriched magnetitite, and (D) gabbro. Normalizing values from Barnes and Maier (1999).

for gabbro in the Upper zone are similar to the undepleted magnetitite patterns but at lower concentrations.

Comparison with Other PGE-Enriched Magnetitite Occurrences

The enrichment of PGE in association with magnetite has been described in other mafic-ultramafic complexes. In the Main Magnetite Layer in the Upper zone of the Bushveld Complex, PGE are concentrated in anorthosite just below the Main Magnetite Layer (Harney et al., 1990; Barnes et al., 2004). However, the magnetite seams themselves contain very little PGE (Barnes et al., 2004). In the Skaergaard intrusion, in Greenland, Pd is concentrated with Cu and Au in anorthositic layers associated with magnetite at the top of the middle zone, having values of up to 3 ppm Pd and 200 ppb Pt (Andersen et al., 1998). In the Rincon del Tigre Complex in Bolivia, Pt and Pd are concentrated with Cu at the base of the magnetite-bearing gabbro in the upper part of the intrusion with maximum precious metals concentrations of 1.8 ppm Pd and 0.68 ppm Pt in separate 1-m samples (Prendergast, 2000).

Pt and Pd are concentrated in magnetitite layers, similar to the Rio Jacaré intrusion, in the Duluth Complex in Minnesota, with values for Birch Lake of 2.7 ppm Pt and 2.5 ppm Pd (Hauck et al., 1997; Nabil, 2003), in the Coldwell Complex in Canada, with values of 1.5 ppm Pd and 0.3 ppm Pt over 1.8 m (Barrie et al., 2002), and in the Stella intrusion of South Africa, with values of up to 7 ppm Pt and 7 ppm Pd (Maier et

TABLE 8. Metal and Sulfur Concentrations in Magnetite-Bearing Rocks

	n	Ni (ppm)	Cu (ppm)	S (ppm)	Ir (ppb)	Rh (ppb)	Pt (ppb)	Pd (ppb)	Au (ppb)	Cu/Pd_{mn}	Ni/Ir_{mn}	Cu/S
Depleted	13	314	1931	1940	0.27	1.24	46	31	37.0	12.31	4.94	0.98
Undepleted	12	306	667	1678	1.05	3.14	176	99	39.0	0.95	1.23	0.51
Enriched	18	379	110	690	1.02	3.13	208	181	15.9	0.11	1.53	0.20

Notes: *n* = number of samples, mn = mantle normalized

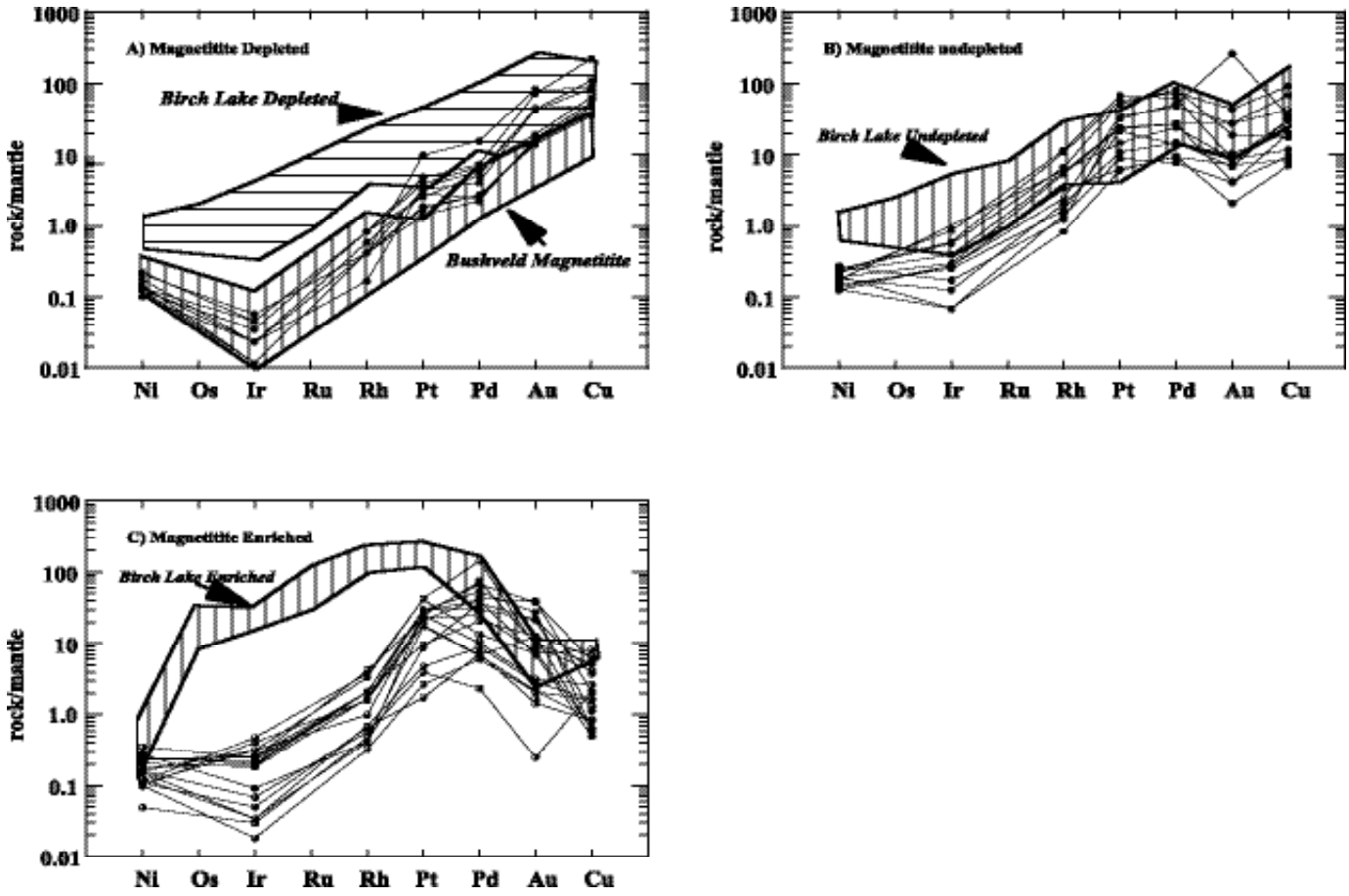

FIG. 9. A comparison of mantle-normalized rock values of Ni, PGE, Au, and Cu for the Rio Jacaré intrusion, with values from other PGE-bearing magnetitite. Values from the Bushveld from Barnes et al. (2004) and for Duluth from Hauck et al. (1996).

al., 2003). In all these intrusions magnetite formed after extensive fractionation of the intrusion.

Samples of oxide layers from the Birch Lake area of the Duluth Complex exhibit PGE-depleted, -undepleted, and -enriched mantle-normalized patterns similar to Jacaré samples (Hauck et al., 1997; Fig. 9). The PGE patterns for Birch Lake and Rio Jacaré are similar from Pt to Au, but the Birch Lake patterns are generally enriched in Os to Rh compared to the Rio Jacaré samples. The Longear, Wyman Creek and Boulder Lake magnetite units of the Duluth Complex also closely resemble the Rio Jacaré depleted and undepleted samples (Nabil, 2003). This comparison suggests that the Rio Jacaré magnetitite is most similar to those found in layered intrusions associated with continental tholeiites. The depleted Rio Jacaré PGE patterns are also similar to those obtained from the northern limb of the Upper zone of the Bushveld (Fig. 9A; Barnes et al., 2004).

The sulfide contents of the Rio Jacaré rocks are very low and the rocks are metamorphosed. This makes the common practice of recalculating the metal values to 100 percent sulfides for the purpose of comparison questionable (Barnes et al., 1988). We show below that sulfur has been mobile in many samples. However, for rocks containing more than 500 ppm sulfur (Table 9) recalculation to 100 percent sulfides shows enrichment in Pt, Pd, Rh, Ir, Au, and Ni but not in Cu, in the magnetitite and magnetite-bearing pyroxenite of the Lower zone compared to the Upper zone. Recalculated sulfide concentrations for samples from Gulçari A are similar to those of PGE-enriched sulfides from Birch Lake (Hauck et al., 1997) and Medvezhy Creek in the Noril'sk Complex (Barnes et al., 1997). In contrast, recalculated sulfide concentrations of the Gulçari B and Novo Amparo samples resemble the PGE-depleted Minnimax sulfides and Dunka Road sulfides of the Duluth Complex (Barnes et al., 1997).

Discussion

Platinum-group element mobility

PGE are known to have different mobilities during alteration by postmagmatic processes. A number of studies have shown that Pd is more mobile than Pt during different types of hydrothermal alteration from syn- to postmagmatic (e.g., Li and Naldrett, 1993) to lower temperature alteration and serpentinization (e.g., Prichard et al., 2001, Seabrook et al. 2004) and weathering (e.g., Fuchs and Rose, 1974, Prichard and Lord, 1994). The occurrence of Pd arsenides, antimonides,

TABLE 9. Metal and Sulfur Concentrations Recalculated to 100 Percent Sulfides

Drill hole	*n*	S (%)	Cu (%)	Ni (%)	Fe (%)	Ir (ppb)	Rh (ppb)	Pt (ppb)	Pd (ppb)	Au (ppb)
Magnetite-bearing rocks										
GA	10	36.08	18.92	5.53	39.47	450	933	85,819	70,692	23,808
NA	14	35.42	28.29	2.74	33.55	201	797	26,746	17,139	5,004
GB	4	38.26	7.17	2.10	52.47	138	595	22,083	12,794	1,064
Gabbro										
GA	4	37.37	9.03	5.45	48.16	139	237	38,700	34,632	4,141
NA	1	35.79	28.99	0.37	34.85	19	74	1,487	743	130
GB	2	36.08	26.63	0.43	36.86	10	34	484	511	130

Notes: *n* = number of samples, only samples with >500 ppm were recalculated to 100% sulfides consisting of chalcopyrite, pentlandite, and pyrhotite; it was assumed that the magnetite contained 200 ppm Ni based on analyses of magnetites from the Bushveld Complex (Klemm et al., 1985); GA = Gulçari A, GC = Gulçari B, NA = Novo Amparo

and tellurides in rows crosscutting magnetite grains in one magnetitite sample suggests some local mobilization of the PGE in the Rio Jacaré intrusion. Also, within the magnetite-bearing pyroxenite, very variable Pt/Pd ratios, from 0.4 to 6.1, and an extreme value of 35 in sample GA41 at a 55-m depth, suggests remobilization of Pt and Pd to different degrees.

However, the much more uniform Pt/Pd ratios in the magnetitite than in the magnetite-bearing pyroxenite, with ratios mainly between 1 and 2 and a range of 0.7 to 3, suggests that the magnetitite was more resistant to alteration and remobilization of the Pt and Pd and that these are magmatic ratios. The close association of the PGE with the magnetite bodies in the Rio Jacaré intrusion also strongly suggests that they were concentrated originally by igneous processes related to magnetite formation. The association of PGM with Ni, Co, Fe, Cu sulfides, sulfarsenides, and alloys supports the idea that sulfur saturation in the magma, which caused the crystallization of base metal sulfides, also caused concentration of PGE within the magnetitite. The PGE may have been present in solid solution in the sulfides or crystallized as discrete PGM. Although metamorphism and alteration have obscured the primary mineralogy, and PGE arsenides, antimonides, and tellurides have been modified by in situ postmagmatic alteration to produce alloys, the evidence from the mineralogical associations of the PGM is in agreement with the geochemistry and suggests that the PGM are still predominantly in their original magmatic positions in the magnetitite.

Processes of magmatic concentration

All of the PGE, Ni, and Cu have high partition coefficients into Fe sulfide liquids (e.g., Peach et al., 1990). Therefore, a potentially important process for concentrating the PGE in the magnetite-rich rocks may have been collection of the PGE from the silicate magma by a sulfide liquid and accumulation of the sulfide liquid in the oxide-rich layers. Capobianco et al. (1994) have shown that the intermediate (I) PGE may be collected by magnetite by concentrating Rh and Ru and excluding Pd. However the magnetitite in the Rio Jacaré intrusion and the magnetite-bearing pyroxenite have similar concentrations of Ir and Rh and of Pt and Pd (Table 7). Therefore, magnetite does not appear to have preferentially collected the IPGE in this case.

The PGE show a good correlation with each other within each drill hole (Figs. 6–7), which suggests that the same phase is controlling them. Copper, S, and Au show similar behavior to the PGE in many samples, but there are many exceptions. If collection of the metals by a sulfide liquid were the only process involved, then the distribution of all of the metals and S would be the same. Therefore, an additional process must be considered. Sulfide liquids formed in equilibrium with mafic magmas normally crystallize as monosulfide solid solution and as intermediate solid solution. At low temperatures, these exsolve chalcopyrite, pentlandite, and pyrrhotite ± pyrite. The Rio Jacaré samples are unusual because chalcopyrite is the most common phase and there is little iron sulfide present. The presence of Cu alloys in some samples and the fact that some samples have Cu/S ratios higher than the Cu/S ratio of intermediate solid solution/chalcopyrite suggests that S has been lost from many of the samples. Cawthorn and Meyer (1993), in their study of the Cu sulfide-bearing magnetite ores of the O'Kiep intrusion in South Africa, suggested that some of the magnetitite ores formed during metamorphism of the igneous sulfides and interaction with oxidizing fluids (e.g., $3FeS + 2O_2 = Fe_3O_4 + 1.5S_2$), resulting in sulfur removal. A similar explanation has been suggested to account for the predominance of chalcopyrite in the sulfide assemblage in chromitite of the Bushveld Complex (e.g., Mathez, 1999; Penberthy and Merkle, 1999). Similar processes could account for the lack of Fe sulfides in the magnetite at Rio Jacaré.

Summary and Conclusions

The Rio Jacaré layered intrusion in northeastern Bahia, Brazil, shows igneous fractionation with increasing Na and K and decreasing Mg and Ca upward through the intrusion. It hosts magnetite-rich units that are rich in vanadium, contain elevated PGE, and show Pt and Pd enrichment in mantle-normalized plots. The PGE correlate with Ni and appear to have been concentrated magmatically within the magnetite bodies. The most common PGM are sperrylite, Pd bismuthides, antimonides, and tellurides, and Pt and Pd alloys. These minerals have been altered in situ with some remobilization especially in the less magnetite-rich rock types. The behavior of PGE in the Rio Jacaré intrusion is similar to a number of other well-known examples of PGE with magnetite.

We propose a model whereby the magma became saturated in oxides and a sulfide liquid at approximately the same time. The PGE, Ni, Au, and Cu were collected by the sulfide

liquid, and the oxide and a small quantity of sulfide liquid collected on the cumulate pile. The sulfides were modified by S loss either during postcumulus processes or metamorphism. The lower sulfur content of the Lower zone magnetitite compared to the Upper zone suggests greater loss of sulfur from the Gulçari A magnetite than the Upper zone magnetitite. The loss of S from a rock with only a little sulfide present will cause the PGE to exsolve from the monosulfide solid solution and, depending on the anions available, PGM containing As, Sb, Te, or Bi may form (e.g., Peregoedova and Ohnenstetter, 2002), and this may account for the abundance of these minerals in the Rio Jacaré magnetitite. Copper and Au were also partially redistributed when the sulfur was remobilized. However the PGE were not significantly mobile, as they all correlate with each other and the PGM have altered in situ.

The PGE enrichments in the Rio Jacaré intrusion are similar to a number of other examples of magnetitite in layered intrusions. The enrichment of PGE in magnetite layers contrasts with the prevailing models for PGE enrichment in layered intrusions. The PGE-rich layers or reefs of the Bushveld Complex, the Stillwater Complex, Great Dyke, and Munni Munni are found in the lower third of the intrusion and were formed relatively early in the crystallization sequence. The oxide with which they are associated is chromite (e.g., Naldrett, 1989). Magnetite layers only occur in the evolved upper parts of the intrusions. Toplis and Carrol (1995) have shown that primary mantle magmas undergo at least 60 percent crystal fractionation before magnetite appears on the liquidus. Thus, magnetite-rich rocks are not generally thought to be good targets for PGE exploration because of the likelihood that PGE have already been removed from the magma by sulfide liquid or PGM crystallization. However, the recent observation of PGE enrichment in a number of occurrences of magnetite-rich layers illustrates that the timing of PGE enrichment depends on when sulfide or PGE saturation occurs, and this can take place relatively late in the crystallization process. Although the majority of the PGE concentrations occur in the lower portions of layered intrusions, the examples of Stella, Rincon del Tigre, and Rio Jacaré suggest that late-stage magnetite-rich layers also may be prospective for PGE if sulfur saturation and conditions favorable for PGE precipitation did not occur until late in the crystallization process.

Acknowledgments

We thank Companhia Baiana de Pesquisa Mineral for access to cores, the Royal Society for support of HMP during this study and the Canadian International Development agency and the Natural Science and Engineering Research Council (NSERC) for financial support for H Sá and S-J. Barnes. R Lechausser is thanked for assistance with PGE and Au analysis. We thank the two referees, C F Filho and L J Cabri, for their helpful and constructive reviews and M. D. Hannington for editing and comments that have improved the paper substantially.

March 14, 2003; October 26, 2004

REFERENCES

Andersen, J.C.Ø., Rassmussen, H., Nielsen, T.E.D., and Rønsbo, J.C., 1998, The Triple group and the Platinova gold and palladium reefs in the Skaergaard intrusion: Stratigraphic and petrographic relations: Economic Geology, v. 93, p. 488–509.

Barnes, S-J., and Maier, W.D., 1999, The fractionation of Ni, Cu and the noble metals in silicate and sulfide liquids: Geological Association Canada Short Course, v. 13, p. 69–106.

Barnes, S-J., Boyd, R., Korneliussen, A., Nilsson, L-P., Often, M., Pedersen, R.B., and Robins, B., 1988, The use of mantle normalization and metal ratios in discrimination between the effects of partial melting, crystal fractionation, and sulfide segregation on platinum-group elements, gold, nickel, and copper: Examples from Norway, *in* Prichard, H. M., Potts, P. J., Bowles, J. F. W., and Cribb, S. J. eds., Geo-platinum symposium volume: London, Elsevier, p. 113–144.

Barnes, S-J., Zientek, M.L., and Severson, M., 1997, Ni, Cu, Au and platinum-group element contents of sulfides associated with intraplate magmatism: A synthesis: Canadian Journal of Earth Sciences, v. 34, p. 337–351.

Barnes, S-J., Maier, W.D., and Ashwal, A.D., 2004, Platinum-group elements distribution in the Main and Upper zone of the Bushveld Complex: Chemical Geology, v. 208, p. 293–317.

Barrie, C.T., MacTavish, A.D., Walford, P.C., Chataway, R., and Middaugh, R., 2002, Contact type and Magnetitite reef-type Pd-Cu mineralization in Ferroan olivine gabbros of the Coldwell Complex, Ontario: Canadian Institute of Mining, Metallurgy and Petroleum Special Volume 54, p. 321–337.

Brito, R.S.C., 1984, Geologia do sill estratificado do Rio Jacaré-Maracás, Bahia: Congresso Brasileiro de Geologia, Sociedade Brasileira Geociências, 9th, Rio de Janeiro, Anais do 33, p. 4316–4334.

——2000, Geologia e petrologia do sill máfico ultramáfico do Rio Jacaré, Bahia e estudo das mineralizações de Fe-Ti-V e platinóides associados: Unpublished Ph.D. thesis, Brasilia, Brazil, Universidade de Brasília, no. 39, 325 p.

Brito, R.S.C., Pimentel, M.M., Nilson, A.A., and Gioia, S.M., 2001, Geology and petrology of the Rio Jacaré Sill, Bahia, Brazil [abs.]: Simpósio de Geologia do Nordeste, 19th, Natal, Resumos, v. 17, p 274–275.

Cabri, L.J., 2002, The platinum-group minerals: Canadian Institute of Mining, Metallurgy and Petroleum Special Volume 54, p. 13–130.

Cabri, L.J., and Laflamme, J.H.G., 1976, The mineralogy of the platinum-group elements from some copper-nickel deposits of the Sudbury area, Ontario: Economic Geology, v. 71, p. 1159–1195.

Capobianco, C.J., Hervig, R.L., and Drake, M.J., 1994, Experiments on Ru, Rh and Pd compatibility for magnetite and hematite solid solutions crystallized from silicate melts: Chemical Geology, v. 113, p. 23–44.

Cawthorn, R.G., and Meyer, F.M., 1993, Petrochemistry of the O' Kiep copper district basic intrusive bodies, northwestern Cape Province, South Africa: Economic Geology, v. 88, p. 590–605.

Feather, C.E., 1976, Mineralogy of the platinum-group elements in the Witwatersrand, South Africa: Economic Geology, v. 71, p. 1399–1428.

Fuchs, W.A., and Rose, A.W., 1974, The geochemical behavior of platinum and palladium in the weathering cycle in the Stillwater Complex, Montana: Economic Geology, v. 69, p. 332–346.

Galvão, C.F., Vianna, I.A., Nonato, I.F.B.P., and Brito, R.S.C., 1986, Depósito de magnetita vanadífera da fazenda Gulçari, Maracás, Bahia, *in* Schobbenhaus, C. and Coelho, C.E.S. eds., Principais depósitos minerais do Brasil: National Department of Mineral Production (DNPM), Brasília, v. 2 (XL), p. 493–501.

Harney, D.M.W., Merkle R.K.W., and Von Gruenewaldt, G., 1990, Platinum-group element behavior in the lower part of the Upper zone of the Eastern Bushveld Complex—implications for the formation of the main magnetite layer: Economic Geology, v. 85, p. 1777–1789.

Hauck, S.A., Severson, M.J., Zanko, L., Barnes, S-J., Morton, P., Alminas, H., Foord, E.E., and Dahlberg, E.H., 1997, An overview of the geology and oxide, sulfide, and platinum-group element mineralization along the western and northern contacts of the Duluth Complex: Geological Society of America Special Paper, v. 312, p. 137–186.

Li, C., and Naldrett, A.J., 1993, High chlorine alteration minerals and Ca-rich brines in fluid inclusions from the Strathcona deep copper zone, Sudbury Ontario: Economic Geology, v. 88, p. 1780–1796.

Maier, W.D., Barnes, S.J., Gartz, V., and Andrews, G., 2003, Pt-Pd reefs in magnetitites of the Stella layered intrusion, South Africa: A world of new exploration opportunities for platinum group elements: Geology, v. 31, p. 885–888.

Marinho, M.M., Vidal, P.H., Alibert, C., Barbosa, J.S.F., and Sabate, P., 1994, Geochronology of the Jequie-Itabuna granulitic belt of the Contendas-Mirante volcano-sedimentary belt: Boletin, Instituto de Geociências, Universidade de São Paulo, v. 17, p. 73–96.

Mathez, E.A., 1999, Magmatic metasomatism and formation of the Merensky reef, Bushveld Complex: Contributions to Mineralogy and Petrology, v. 119, p. 277–286.

Nabil, H., 2003, Genese de deposits de Fe-Ti-P associes aux intrusions litees (ecemples: Complexe de Sept Iles, au Quebec; Complexe de Duluth aux Etats-Unis: Unpublished Ph.D. thesis, Chicoutimi, Université du Quebec, 440 p.

Naldrett, A.J., 1989, Magmatic sulfide deposits: New York, NY, Oxford University Press, 189 p.

Peach, C., Mathez, E.A., and Keays, R.R., 1990, Sulfide melt-silicate melt distribution coefficients for noble metals and other chalcophile elements as deduced from MORB: Implications for partial melting: Geochimica et Cosmochimica Acta., v. 54, p. 3379–3389.

Penberthy, C.J., and Merkle, R.K.W., 1999, Lateral variations in the platinum-group element content and mineralogy of the UG-2 chromitite layer, Bushveld Complex: South African Journal of Geology, v. 102, p. 240–250.

Peregoedova, A., and Ohnenstetter, M., 2002, Collectors of Pt, Pd and Rh in an S-poor Fe-Ni-Cu-sulfide system at 760°C: Experimental data and application to PGE deposits [abs.]: IGCP 427, International Platinum Symposium, 9th, Billings, Montana, July 2002, Abstract Volume, p. 367–370.

Prendergast, M.D., 2000, Layering and precious metals mineralization in the Rincon del Tigre Complex, eastern Bolivia: Economic Geology, v. 95, p. 113–130.

Prichard, H.M., and Lord, R.A., 1994, Evidence for the mobility of PGE in the secondary environment in the Shetland ophiolite complex: Transactions of the Institution of Mining and Metallurgy, v. 103B, p. B79–B86.

Prichard, H.M., and Tarkian, M., 1988, Pt and Pd minerals from two PGE-rich localities in the Shetland ophiolite complexes: Canadian Mineralogist, v. 26, pt. 4, p. 979–990.

Prichard, H.M., Sà, H., and Fisher, P.C., 2001, Platinum-group mineral assemblages and chromite composition in the altered and deformed Bacuri Complex, Amapa, northeastern Brazil: Canadian Mineralogist, v. 39, p. 377–396.

Robert, R.V.D., Van Wyk, E., Palmer, R., and Steele, T.W. 1971, Concentration of the noble metals by fire assay technique using nickel-sulfide as a collector: National Institute for Metallurgy, South Africa, Report 1371, 20 p.

Sá, J.H.S., 1985, Pesquisa de platinoides no complexo do rio Jacaré: Internal report, Bahia, Brazil, Companhia Baiana de Pesquisa Mineral, 9 p.

——1992, Feições petroquímicas relacionadas a estrutura do corpo Gulçari A no complexo máfico-ultramáfico do Rio Jacaré, Maracás, Bahia [abs.]: 37º Congresso Brasileiro do Geologia, São Paulo, Botetim de Resumos Expandidos, p. 460–462.

Seabrook, C.L., Prichard, H.M., and Fisher, P.C., 2004, Platinum-group minerals in the Raglan Ni-Cu-(PGE) sulfide deposit, Cape Smith, Canada: Canadian Mineralogist, v. 42, p. 485–497.

Teixeira, W., Sabaté, P., Barbosa, J., Noce, C.M., and Carneiro, M.A., 2000, Archean and Paleoproterozoic tectonic evolution of the São Francisco craton: International Geological Congress, 31st, Rio de Janeiro, Brazil, August 6–17, 2000, Proceedings, p.101–137.

Toplis, M.J., and Carrol, M.R., 1995, An experimental study of the influence of oxygen fugacity on Fe-Ti oxide stability, phase relations, and mineral-melt equilibria in ferro-basaltic systems: Journal of Petrology, v. 36, p. 1138–1170.